DESIGN AND PROCESS CONSIDERATIONS FOR EFFECTIVE ADDITIVE MANUFACTURING OF HEAT EXCHANGERS

Evan Handler[1], Amanda Sterling[2], Jonathan Pegues[2], Huseyin Ozdes[2], Mohammad Masoomi[2], Nima Shamsaei[2], Scott M. Thompson[2,†]

[1]Naval Surface Warfare Center, Carderock Division, Potomac, MD 20817 USA

[2]Laboratory for Fatigue and Additive Manufacturing Excellence, Department of Mechanical Engineering, Auburn University, AL 36849 USA

† Corresponding author:
Email: smthompson@auburn.edu
Phone: (334) 844 4867

Abstract

This paper provides some insights into using powder bed fusion (PBF) techniques for additively manufacturing heat transfer equipment (HTE), such as heat pipes and heat sinks. Background information is provided on the operating principles of PBF and the subsequent features of parts fabricated via PBF. Examples of heat transfer equipment produced using PBF are discussed. Some benefits and challenges associated in using PBF for generating effective heat transfer equipment are summarized.

Introduction

In recent years, there has been interest in using powder bed fusion (PBF) for the additive manufacture (AM) of heat transfer equipment (HTE). PBF methods provide several advantages over traditional manufacturing methods in this area. The most commonly claimed advantage is its ability to create objects with geometries once impossible to create with traditional manufacturing processes. PBF enables the ability to create complex internal structures in a single manufacturing step, whereas most heat exchangers that are designed with internal structures must be assembled using various joining methods that can cause thermal resistance and decrease heat transfer rates.

While there are many different types of HTE, they all generally encounter similar challenges in the manufacturing process. One example is the issue of thermal resistance between adjoined surfaces, which typically is caused by small gaps between the surfaces, though the issue also is present when two surfaces are joined using traditional joining methods. Furthermore, since research related to the design of THE is often done computationally to create highly-optimized designs [1], computer-generated designs sometimes can be impractical or even impossible to manufacture. Furthermore, as miniaturization becomes increasingly prevalent, careful consideration must be given toward manufacturing methods required for parts. Thus, for every advance made in thermal management devices, its benefit must be weighed against the cost of manufacturing and implementing new components.

The AM of a part is accomplished through guidance of a CAD file and by adding material continuously, in a layer by layer fashion, until a finished product is produced in a usable or near usable state. Among the different AM techniques, PBF has become the most commonly researched and used technique. PBF works by using a moving heat source that is supplied either by a laser or an electron beam. The heat source is controlled by computer numerical control (CNC) to melt specific areas in a bed of metallic powder to form a single layer. Then, the build stage is lowered, and another layer of powder is coated on top of the previous layer; this process is repeated until the final part is produced. Laser-based PBF is sometimes referred to as laser-powder bed fusion (L-PBF) selective laser melting (SLM) or direct metal laser sintering (DMLS).

PBF has several advantages over other metal-based AM methods, including smaller layers, finer details, and the ability to create internal structures without supports over the previous layers of unmelted powder. PBF has been shown to be effective in producing parts with a wide variety of metal alloys, including many different titanium-, steel-, aluminum-, nickel- and commercially pure copper-based alloys [6,7]. In industry, PBF has been used successfully to create various parts, such as the fuel injector for a new General Electric (GE) jet engine [4], a copper combustion chamber for NASA [5], and even biocompatible tissue scaffolds [6].

Surface Roughness

PBF methods are known to produce rough surfaces on manufactured parts. Under many circumstances, these surfaces are either machined or sandblasted to make the surfaces smoother, but some researchers have chosen to study the roughness of the surfaces with the goal of finding ways to reduce or prevent it. While rough surfaces are undesirable in structural and moving parts that undergo fatigue, they can be both a benefit and a hindrance in heat exchangers. For example, roughness has been shown to increase heat transfer by causing more local turbulence in the working fluids and providing more surface area, but it also has been shown to increase the pressure drop across surfaces.

Rough surfaces are a direct result of the PBF process, and they can be caused by various mechanisms. The most visible surface roughness is caused by the successive, partially-overlapping passes of the heat source, which causes successive, visible grooves between the path of the heat source and the successive layers. This is due to the influence of surface tension, which causes the top of the molten pool to take a spherical shape. Furthermore, early in the process, this effect of surface tension can cause some molten particles to “splash” (or spatter) and then solidify as much smaller particles if they land on a previously-melted section. It is common for the surfaces of particles just outside the melt pool to partially melt and become sintered to the part as the heat source moves away [7]. An example of the surface roughness inherent to PBF surfaces/channels is shown in Fig. 1 which shows a channel structure next to a milled surface. The surface was milled to visualize mini-channel surface roughness within a PBF/Ti-6Al-4V flat oscillating heat pipe [8].

Most studies have indicated that surface roughness is dominated, in large part, by the process parameters that exist when the basic samples are produced. Hatch spacing directly influences the distance between grooves, and lower hatch spacing decreases this distance [16-18]; the thickness of the layers causes a similar effect in the z direction, although this does not occur in DMLS [9]. The direction in which the surface roughness builds is another important

factor because vertical and horizontal surfaces will have drastically different surface roughnesses [17,19]. Scan velocity and the power of the heat source have been shown to have some influence on surface roughness because they influence both the heating rate and subsequent cooling rate, but these influences are not always significant [17, 18, 20]. The size of the particles that make up the powder and their size distribution have significant effects on surface roughness; smaller particle sizes and smaller size distributions in the powder decrease surface roughness [16, 21]. The extent to which all these parameters effect surface roughness varies based on the method and the material used. Some parameter optimization studies have attempted to determine sets of parameters that result in the lowest surface roughness. Calignano et al. [12] investigated the effects of different SLS process parameters on the surface roughness of AlSi10Mg, and they used the Taguchi method to determine an ideal set of parameters for the best surface roughness. Optimal parameters were chosen based on this analysis, and the samples that were produced using these parameters were found to have an average surface roughness of Ra = 15.68 μm.

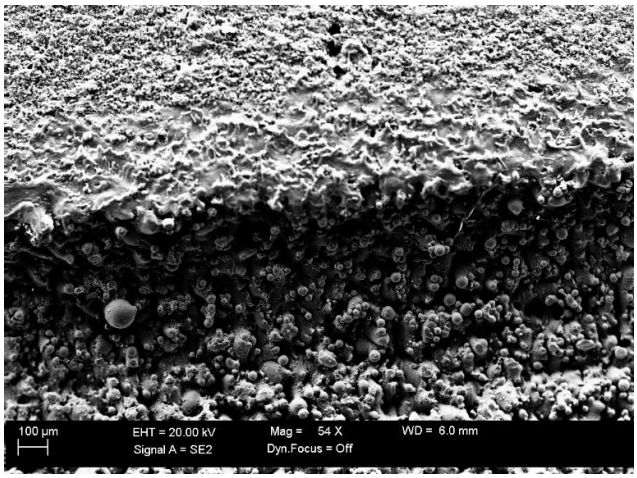

Figure 1. SEM image of a PBF/Ti-6Al-4V mini-channel adjacent to a machined surface.

The geometrical orientation of the part during its AM has a substantial influence on surface roughness, especially when complex geometries are involved. Pakkanen et al. [14] studied this phenomenon using SLM to produce variations of tubing 10 mm thick out of AlSi10Mg and Ti-6Al-4V. The AlSi10Mg tubes were produced at various angles between the horizontal and vertical orientations, while the Ti-6Al-4V tubes were produced only at an angle of 45º. The tubing samples were cut in half, and surface roughness measurements were taken from the top and bottom of the internal channels for comparison. All cases were found to have Ra values of 20 μm with an error of ±5 μm.

There are other phenomena and circumstances that affect surface roughness in different ways. For example, Jamshidinia et al. studied the effect of heat buildup on surface roughness in EBM by producing sets of two thin walls made of Ti-6Al-4V with different spacing between them [15]. They found that lower heat accumulation resulted in lower roughness values, and they also found that there was an approximate logarithmic relationship between the spacing distance and surface roughness. Wang et al. used SLM to produce curved overhang structures out of SS 316L with different laser power settings to study the surface roughness of both the top and bottom surfaces as the incline angle increased [16]. They found that surface roughness began to increase sharply when the incline angle exceeded 45º for both surfaces. Distinct changes in the

surfaces were observed on all samples as they transitioned from fully dense and successful to build failure.

Porous Structures

Porous materials often are used in heat pipes as wicking structures, often implemented through metal foams or sintering processes. However, many 'traditional' porous foams involve a high degree of randomness, and their effectiveness cannot always be considered optimal. In comparison, PBF methods provide an opportunity to manufacture porous structures with pre-optimized designs for more efficient HTE. The work of Bodla et al. numerically showed that well-designed artificial porosity can produce significant increases in effective heat transfer over other traditionally-produced materials [17]. The production and use of cellular lattice structures have been investigated. These are beneficial in increasing heat transfer due to their high surface area and continuous nature. To date, many different types of cells have been additively manufactured successfully, and much work has been done to investigate the manufacturability of different volume fractions and the changes in the strut and pore sizes [31 - 33]. Some shapes have been tested and confirmed to have higher effective heat transfer coefficients than those in otherwise porous materials [20]. The design of these structures currently is limited by the minimum producible feature size [20].

Heat Sinks

Wong et al. used SLM to produce heat sink arrays of Al 6061 and some SS 316L with different geometries to compare their associated heat transfer and pressure drop during cross-flow of air through the arrays [34 - 36]. The geometrical shapes that were produced included cylindrical, rectangular, diamond-shaped, and elliptical pins, as well as an alternating "V" array and a lattice array – with an example of the lattice array shown in Fig. 2. In all of the studies, the heat sinks were manufactured on a 50 x 100-mm substrate of the same material used in the production of the fins. Testing was performed using a 16-mm copper block heated by two 6-mm diameter electrical cartridge heaters bolted to the bottom surface of the heat sinks. Ambient air was forced through piping at varying velocities, and the lengths of the pipes were designed for fully-developed conditions both before the heat sink and before the final measurements were taken. The heated section was fully insulated. For comparison, pressure and temperature were measured before and after the heat sink. In all cases, surface roughness was estimated to be between 15-25 μm.

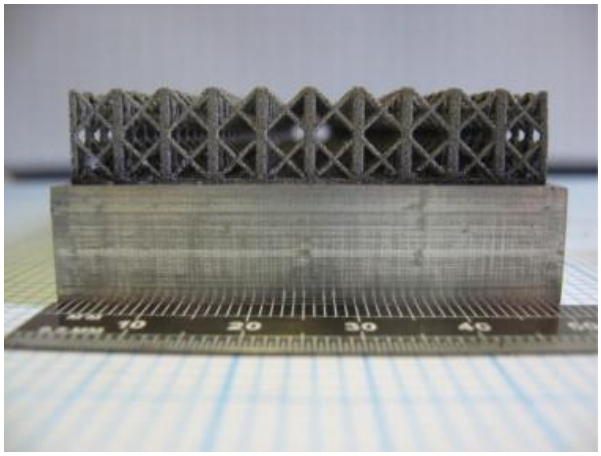

Figure 2. Lattice-structured heat sink fabricated via L-PBF [34]. *Used with permission*.

When SS 316L heat sinks were tested, their performances were only about half those of the Al 6061 heat sinks due to the poor thermal conductivity of SS 316L [23]. When the different geometries were compared, the cylindrical pins and the "V-shaped" array performed roughly the same at equal Reynolds numbers, and the diamond-shaped pins produced significantly higher heat transfer at much lower Reynolds numbers, while the elliptical pins produced the lowest heat transfer. However, the cylindrical pins resulted in a nearly constant pressure drop, and the diamond-shaped pins initially created higher pressure drops that decreased as Reynolds number increased. The "V-shaped" array produced significantly lower pressure drops that decreased as Reynolds number increased until eventually leveling out, and the elliptical pins fell roughly in the middle [36, 37]. These results changed when rectangular pins and lattice structures, modified cylindrical pin dimensions, and modified elliptical pin dimensions were tested. With better dimensions, the rectangular and elliptical pins were found to have similar heat transfer when tested at the same flow rates, but the cylindrical pins still were inferior. However, the lattice structure had significantly lower heat transfer even though it had a larger surface area. This was due in part to the fact that the lattice was designed to have channels that allow air flow with little interaction with the lattice structure, and this reduces heat transfer. When the pressure drops were compared, the elliptical pins produced the lowest pressure drops, the cylindrical pins produced the highest, and the pressure drops for the rectangular pins and lattice structure were about the same.

Dede et al. used 3D topology optimization methods to generate a geometry file for a pin-based heat sink, which was manufactured by SLM using AlSi12 [1]. **Error! Reference source not found.** shows the CAD geometry of this optimized heat sink. Then, the printed heat sink was tested against heat sinks made out of Al 7075 and oxygen free Cu and produced using traditional manufacturing techniques. These heat sinks were tested using air jet infringement, and the pressure drops and air temperatures were recorded. The heat sinks were mounted to a heater, which was backed by PEEK insulation.

During the experiments, the air flow rate was set and the heater was ramped up until there was a temperature difference of 15 K between the heater and the average temperature of the surface-mounted thermocouples. The system was allowed 30 min to reach steady state before the temperatures and pressure drops were recorded. The temperature and pressure data were used to

calculate the thermal resistance. Two different cases were studied, and the first case used all aluminum heat sinks, and the data were gathered using a jet flow rate between 5-20 cubic feet/min (CFM). In this case, the optimized heat sink had a thermal resistance of 0.72 ºC/W, which was lower than all of the other heat sinks except for one that had a thermal resistance of 0.6 ºC/W, although it also had a significantly higher pressure drop.

A comparison of COP, was used, and it was found that the printed heat sink, , with a COP of 2.37, had a significant advantage over all of the other heat sinks that were tested. In the second case, the optimized heat sink was tested against the copper heat sinks using flow rates between 5-15 CFM. In this case, the optimized heat sink had a lower thermal resistance than two of the copper heat sinks, but the third copper heat sink had the lowest thermal resistance, i.e., 0.249 °C/W. However, it was found that the thermal resistance of this copper heat sink had been decreased because its pressure drop was significantly higher than that of the printed heat sink. In this case, the optimized heat sink was again found to have the highest COP value, i.e., 0.197.

Heat Pipes

Thompson et al. used L-PBF to produce multi-layered, flat-plate oscillating heat pipes (FP-OHPs) which are typically used in high heat flux applications [8]. The FP-OHPs had a total volume of 5.08 × 3.81 × 1.58 cm^3, and consisted of a closed loop, serpentine-arranged mini channel with a diameter of 1.52 mm. A fill port was attached to the side for adding/removing working fluid as necessary. **Error! Reference source not found.** shows a schematic and photograph of the FP-OHP. Nine "vent holes" were integrated into the design to remove any powder that was trapped in the channels, which was done by repeatedly flushing the channels with acetone. Excess powder was brushed off of all exterior surfaces and the top and bottom surfaces were milled to give a smooth finish.

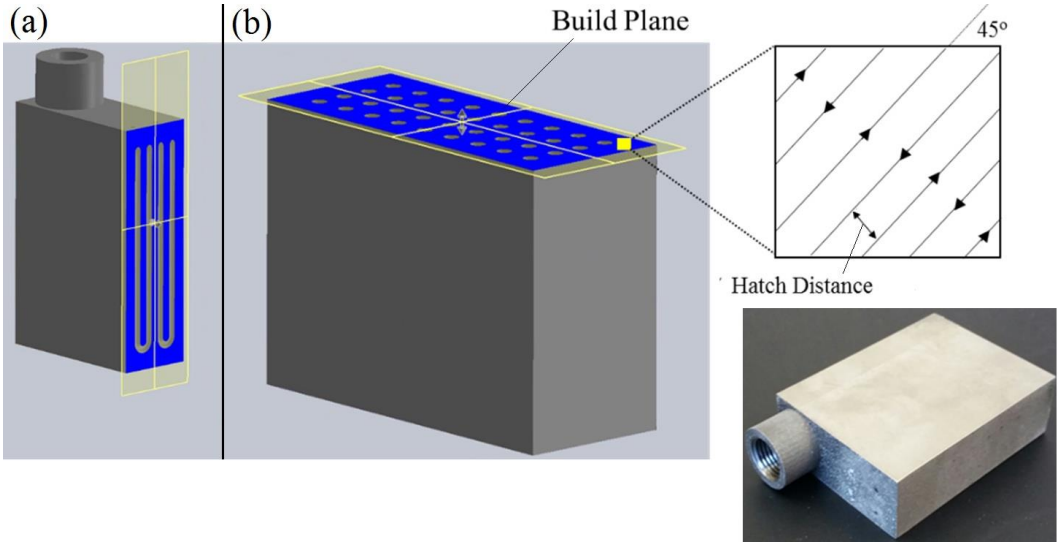

Fig. 3. The FP-OHP with build plane (a) shown relative to fill port and (b) relative to powder bed including the laser path directions and hatch distance. Photograph of finished Ti-6Al-4V also shown [8]. *Used with permission.*

The FP-OHPs were tested and found to operate successfully in both the horizontal and vertical conditions. It was found that critical power inputs were required to initiate the operation of the OHPs, i.e., between 15-20 W for the vertical operation and between 20-25 W for the horizontal orientation. Effective thermal conductivities were calculated at different powers for both orientations, and found to be approximately the same at 45 °C, i.e. k = 110 W/m-K. This was roughly 500% higher than a solid block of Ti-6Al-4V, while the empty pipe had keff = 18 W/m-K.

Summary

Although there is evidence supporting the case for using PBF to manufacture HTE, there are still significant obstacles and challenges that must be overcome and potential research avenues that have yet to be explored. For example, many of the materials and alloys typically used for HTE are not readily manufacturable using PBF, e.g. pure copper and aluminum. Furthermore, although there is much interest in designing internal features, the very nature of PBF will leave any internal feature full of powder, and removal would require either special design considerations or physical drilling into the structure and plugging the hole afterwards [8]. Furthermore, there appear to be limitations on the minimum size of any feature that can be produced due to powder size availability. However, one of the biggest opportunities for merging PBF and THE is the ability to design and manufacture highly-conformal parts with thermal management already integrated into them. This could lead to significantly more efficient heat transfer in less space, because it would eliminate the need for external heat exchangers and completely eliminate the thermal resistance between the heat source and the heat exchanger.

Acknowledgments

This work was sponsored in part by the National Science Foundation under Grant# ECCS 1660446.

References

[1] Dede, E. M., Joshi, S. N., and Zhou, F., 2015, “Topology Optimization, Additive Layer Manufacturing, and Experimental Testing of an Air-Cooled Heat Sink,” J. Mech. Des., **137**(11), p. 111403.

[2] Yap, C. Y., Chua, C. K., Dong, Z. L., Liu, Z. H., Zhang, D. Q., Loh, L. E., and Sing, S. L., 2015, “Review of selective laser melting: Materials and applications,” Appl. Phys. Rev., **2**(4), p. 41101.

[3] Frazier, W. E., 2014, “Metal additive manufacturing: A review,” J. Mater. Eng. Perform., **23**(6), pp. 1917–1928.

[4] Kellner, T., 2015, “The FAA Cleared the First 3D Printed Part to Fly in a Commercial Jet Engine from GE - GE Reports.”

[5] McMahan, T., and Harbaugh, J., 2015, “NASA 3-D Prints First Full-Scale Copper Rocket Engine Part.”

[6] Shishkovsky, I. V, Volova, L. T., Kuznetsov, M. V, Morozov, Y. G., and Parkin, I. P., 2008, “Porous biocompatible implants and tissue scaffolds synthesized by selective laser sintering from Ti and NiTi.”

[7] Song, Y.-A., “Experimental Study of the Basic Process Mechanism for Direct Selective Laser Sintering of Low-Melting Metallic Powder.”

[8] Thompson, S. M., Aspin, Z. S., Shamsaei, N., Elwany, A., and Bian, L., 2015, “Additive manufacturing of heat exchangers: A case study on a multi-layered Ti–6Al–4V oscillating heat pipe,” Addit. Manuf., **8**, pp. 163–174.

[9] Delgado, J., Ciurana, J., and Rodríguez, C. A., “Influence of process parameters on part quality and mechanical properties for DMLS and SLM with iron-based materials.”

[10] Sachdeva, A., Singh, S., and Sharma, V. S., 2013, “Investigating surface roughness of parts produced by SLS process,” Int. J. Adv. Manuf. Technol., **64**(9–12), pp. 1505–1516.

[11] Wang, Y., Bergström, J., and Burman, C., 2006, “Characterization of an iron-based laser sintered material,” J. Mater. Process. Technol., **172**(1), pp. 77–87.

[12] Calignano, F., Manfredi, D., Ambrosio, E. P., Iuliano, L., and Fino, P., 2013, “Influence of process parameters on surface roughness of aluminum parts produced by DMLS,” Int. J. Adv. Manuf. Technol., **67**(9–12), pp. 2743–2751.

[13] Spierings, A. B., Herres, N., and Levy, G., 2011, “Influence of the particle size distribution on surface quality and mechanical properties in AM steel parts,” Rapid Prototyp. J., **17**(3), pp. 195–202.

[14] Pakkanen, J., Calignano, F., Trevisan, F., Lorusso, M., Ambrosio, E. P., Manfredi, D., and Fino, P., 2016, “Study of Internal Channel Surface Roughnesses Manufactured by Selective Laser Melting in Aluminum and Titanium Alloys,” Metall. Mater. Trans. A, **47**(8), pp. 3837–3844.

[15] Jamshidinia, M., and Kovacevic, R., 2015, “The influence of heat accumulation on the surface roughness in powder-bed additive manufacturing,” **3**(1).

[16] Wang, D., Mai, S., Xiao, D., and Yang, Y., 2016, “Surface quality of the curved overhanging structure manufactured from 316-L stainless steel by SLM,” **86**(1–4), pp. 781–792.

[17] Bodla, K. K., Garimella, S. V., and Murthy, J. Y., 2014, “3D reconstruction and design of porous media from thin sections,” Int. J. Heat Mass Transf., **73**, pp. 250–264.

[18] Yan, C., Hao, L., Hussein, A., Bubb, S. L., Young, P., and Raymont, D., 2014, “Evaluation of light-weight AlSi10Mg periodic cellular lattice structures fabricated via direct metal laser sintering,” J. Mater. Process. Technol., **214**(4), pp. 856–864.

[19] Yan, C., Hao, L., Hussein, A., Young, P., and Raymont, D., 2014, “Advanced lightweight 316L stainless steel cellular lattice structures fabricated via selective laser melting,” Mater. Des., **55**, pp. 533–541.

[20] Takezawa, A., Kobashi, M., Koizumi, Y., and Kitamura, M., 2017, “Porous metal produced by selective laser melting with effective isotropic thermal conductivity close to the Hashin–Shtrikman bound,” Int. J. Heat Mass Transf., **105**, pp. 564–572.

[21] Wong, M., Owen, I., Sutcliffe, C. J., and Puri, A., 2009, “Convective heat transfer and pressure losses across novel heat sinks fabricated by Selective Laser Melting,” Int. J. Heat Mass Transf., **52**(1), pp. 281–288.

[22] Wong, M., Owen, I., and Sutcliffe, C. J., 2009, “Pressure Loss and Heat Transfer Through

Heat Sinks Produced by Selective Laser Melting," Heat Transf. Eng., **30**(13), pp. 1068–1076.

[23] Wong, M., Tsopanos, S., Sutcliffe, C. J., and Owen, I., 2007, "Selective laser melting of heat transfer devices," Rapid Prototyp. J., **13(**5), pp. 291–297.